Identification of the material parameters of soft tissues in the compressed leg.

Laura Dubuis, Stéphane Avril, Johan Debayle, Pierre Badel

RESEARCH ARTICLE

Identification of the material parameters of soft tissues in the compressed leg

L. Dubuis, S. Avril, J. Debayle and P. Badel*

Center for Health Engineering, École des Mines de Saint-Étienne, Saint-Étienne, France

(*Received 00 Month 200x; final version received 00 Month 200x*)

Elastic compression is recommended in prophylaxis and treatment of venous disorder of the human leg. However, the mechanisms of compression are not completely understood and the response of internal tissues to the external pressure is partially unknown. To address this later issue, a 3D FE model of a human leg is developed. The geometry is derived from 3D CT-scans. The FE model is made up of soft tissues and rigid bones. An inverse method is applied to identify the properties of soft tissues which are modelled as hyper-elastic, near-incompressible, homogeneous and isotropic materials. The principle is to calibrate the constitutive properties by using CT-scans performed with and without the presence of a compression sock. The deformed geometry computed by the calibrated FE model is in agreement with the geometry deduced from the CT-scans. The model also provides the internal pressure distribution, which may lead to medical exploitation in the future.

Keywords: soft tissues; elastic compression; mechanical identification; FE model; constitutive properties

1. Introduction

The function of venous system is to return the blood from the organs to the heart. To help this function, valves located along the veins prevent the back flow of venous blood. However gravitational forces significantly affects the venous return: when a person is standing or sitting for example, the presence of valves alone is not sufficient to force blood out of the leg. This may result in a build up of hydrostatic pressure due to the weight of the fluid and cause vein dilatation. Without the operation of an important compensatory mechanism, standing upright would lead to a significant oedema. Indeed the venous return from the leg is underpinned by the muscular contraction which drains off stagnant blood from the muscles and deep veins. Accordingly the calf is commonly called the peripheral heart: it fills up and empties repeatedly. People suffering from venous diseases or subject to prolonged standing position may suffer from irreversible damage in their valves. This leads to varicose vein or oedema in more serious cases.

The recommended treatment for venous insufficiency is to wear elastic compression (EC) garments. Though the contribution of EC is shown to be clinically efficient (Amsler et al. 2009; Musani et al. 2010; Oduncu et al. 2004), the actual mechanisms of EC and its biomechanical effects on internal tissues are still partially unknown. Studies found in the literature approach the problem in three different ways.

*Corresponding author. Email: badel@emse.fr

The first one is to model the contact between the sock and the leg (Gaied et al. 2006; Dai et al. 2007; Li et al. 2003; You et al. 2007; Zhang et al. 2007). The motivation behind this comes from the observation that the increase of the intramuscular pressure is either lower or higher than the pressures measured between the skin and the sock at the middle of the calf (Maton et al. 2006). This discrepancy is due to the fact that the pressure exerted by socks is not uniform around the leg.

The second approach to solve this problem is to model the blood flow in veins (Aubert et al. 2001; Downie et al. 2008; Cros et al. 2002; van Donkelaar et al. 2001; Guesdon et al. 2007).

The third approach is to model the compressed soft tissues in a patient specific way. In these studies, biological soft tissues are usually assumed to be hyper-elastic. By performing medical imaging and applying inverse methods, the material properties of soft tissues can be identified. This procedure was followed respectively by Oomens et al. (2003); Linder-Ganz et al. (2007) and Avril et al. (2010); Bouten (2009) to determine the material properties of the buttock and of the leg. In such studies, natural mechanical loading is used to identify constitutive parameters. Finite element (FE) models of the undeformed tissues are constructed from medical images of the non-compressed tissues. A second set of images taken in the compressed state is used to determine the constitutive properties fed into the FE model for calibration purposes (Avril et al. 2010; Linder-Ganz et al. 2007). The calibrated model gives access to the internal pressure distribution of the patient-specific leg. This approach is generally applied for 2D FE models. The aim of this study is to extend it to 3D FE modelling of the human leg under EC.

This paper is focused on the identification methodology. The medical exploitation of the results is out of scope.

2. Methods

2.1 Protocol

3D Computed Tomography scans (CT scans) of the right leg are acquired on a 25 year old female volunteer without venous pathology, following informed consent and according to a protocol approved by the local institutional ethics committee. The scans are acquired with and without EC in a seated position. The compression sock used is the BVSport© *Pro Recup* sock. This sock, specifically designed for recovering after sport exercising efforts (Couzan et al. 2009), applies maximum compression at the calf instead of the ankle as is the case of traditional compression socks. The pressure increases linearly from ankle (0.6 kPa in mean) to knee (4.7 kPa in mean).

In order to evaluate the actual pressure applied locally onto the leg, the stiffness of the sock must be characterized. Consequently, the sock used in the first place during the image acquisition is subsequently tested in tension at different heights. A non-destructive system based on the NF G30-102 standard (AFNOR 1986) is used to reproduce loading conditions similar to those observed when the sock is worn. The textile fibres in the weft direction are aligned to the loading direction throughout the whole test. The fabric stiffness k is deduced at different heights as the average slope of the tension *versus* strain curve. It is estimated with an accuracy of 14%. The set-up is shown in Figure 1. The obtained values are used for setting the boundary conditions of the model (see section 2.3).

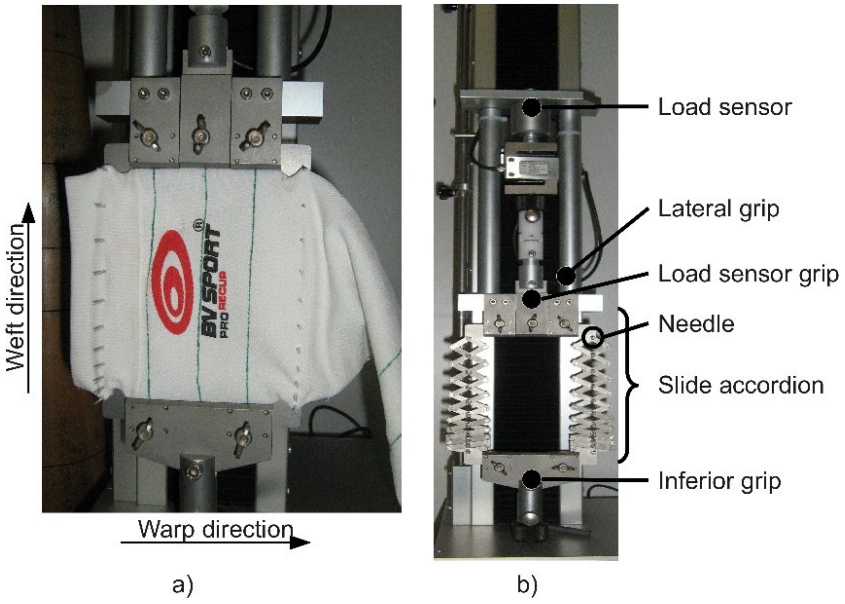

Figure 1. Tensile test of the socks: (a) unloading state and (b) loading state. Lateral needles and slide accordion are used to prevent the sock from stretching in the warp direction, which is close to the actual deformation.

2.2 Geometry and meshing

2.2.1 Image acquisition and processing

The size of the CT-scan images is $512 \times 512 \times 376$ voxels and the voxel size is $0.93 \times 0.93 \times 1$ mm. A cylindrical coordinate system (r, θ, z) is defined, z being the vertical axis (Figure 2) obtained by diagonalizing the inertia matrix of the mechanical system composed of the tibia and fibula bones. The inertia matrix is computed from the 3D images. After different steps of image processing (filtering, thresholding and cleaning), the images are segmented into three regions:

- region one is composed of the adipose tissue (skin and fat) and some veins,
- region two is composed of the muscles, blood vessels, tendons and fasciae,
- region three is composed of the tibia and fibula bones of the leg.

These regions are shown on Figure 2. Segmentation is performed using the ImageJ software.

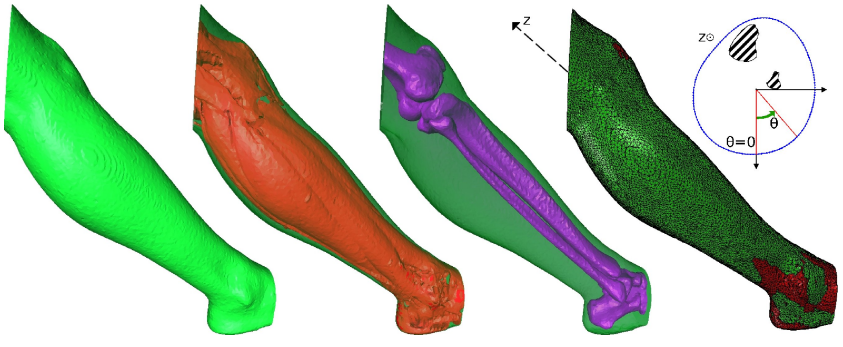

Figure 2. Segmented images (exterior boundary, muscle boundary, bones boundary) and mesh.

2.2.2 Mesh generation and element type

Once the 3D medical images have been segmented, the Avizo© software is used to generate the mesh. 359,374 tetrahedral elements (71,960 nodes) were used to

create the FE model. There are three quality criteria for the surface mesh:

(1) the aspect ratio (< 10), defined as the ratio of the radii of the circumcircle and the incircle for each triangle.
(2) the dihedral angle ($> 11°$), defined as the angle between each pair of adjacent triangles at their common edge.
(3) the tetra quality ratio (< 20), defined as the ratio of the radii of the circumsphere and the inscribed sphere for the tetrahedron which would probably be created.

For fulfilling the quality criteria, the surface mesh is smoothed. At each eight z, a five-degree-Fourier descriptor of the contour is defined according to:

$$r(\theta, z) = a(z) + \sum_{j=1}^{5} [b_j(z)\cos(j\theta) + c_j(z)\sin(j\theta)] \quad (1)$$

where $(r(\theta, z), \theta)$ are the cylindrical coordinates of the smoothed contour at the height z and a, b_j, c_j are the coefficients of the Fourier descriptor. The coefficients are obtained by fitting in the least squares sense the original nodes located in a layer of 5 mm thick centred in z. Knowing that the nodes of the surface to be smoothed are located with their angle θ_i in the cylindrical coordinate system, their new radii computed from the Fourier descriptors are $r(\theta_i, z_i)$. Fourier descriptors are commonplace for describing closed curves (van Kaick et al. 2010; Zahn and Roskies 1972).

The tetramesh is created from the smoothed surface mesh and is exported to the Abaqus© software for FE computations.

The elements of the soft tissues are hybrid tetrahedral linear elements (6.9 Abaqus 2009; Fung and Tong 2001).

2.3 Boundary conditions of the FE model

All the degrees of freedom along the contours of the tibia and fibula bones are fixed, as they are assumed to be infinitely rigid (their elastic properties are nearly 1000 times as large as those of soft tissues). An inhomogeneous pressure is applied on the external surface of the leg. On this surface, positions are fully defined by their coordinates θ and z in the global cylindrical coordinate system. At a given position (θ, z), the value of the local pressure is obtained from the Laplace law:

$$P(\theta, z) = \frac{T(z)}{R(\theta, z)} = k(z)\frac{\varepsilon(z)}{R(\theta, z)} \quad (2)$$

where P is the pressure, T the sock tension, R the local curvature radius of the leg in the horizontal plane (curvature in the vertical plane is neglected), k the fabric stiffness, and ε the local sock strain. The latter is derived from the known perimeters of the leg and of the sock: $\varepsilon = \frac{l - l_0}{l_0}$ where l is the perimeter of the leg and l_0 the perimeter of the sock. The perimeters of the sock are measured and those of the leg are estimated from the CT-scans.

The fabric stiffness is measured at the sock ankle and calf according to the method described in section 2.1. The value of k depends only on the vertical coordinate, *i.e.* it is constant in horizontal planes. It is also constant from the ankle to a height of 60 mm above the ankle, then increases linearly up to a height of 140 mm and is constant again in the calf region (Figure 3).

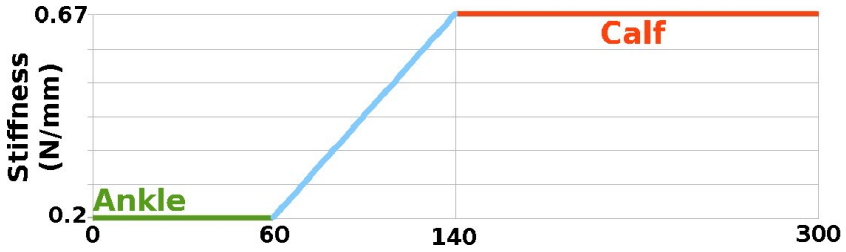

Figure 3. Sock stiffness as a function of height.

The Fourier descriptors used to smooth the surface mesh (Equation 1) are also used to compute the local curvature radius which is required in the Laplace law (Equation 2). Each node i is defined by its angle and its height (θ_i, z_i) in the cylindrical coordinate system. The radius of the contour at the height z_i is a function of the angle: $r = r(\theta, z_i)$. The first and second derivatives of $r(\theta, z_i)$ with respect to θ are used to compute the local curvature radius $R(\theta, z_i)$ according to:

$$R(\theta, z_i) = \frac{\left(r^2(\theta, z_i) + r'^2(\theta, z_i)\right)^{\frac{3}{2}}}{r^2(\theta, z_i) + 2r'^2(\theta, z_i) - r(\theta, z_i)r''(\theta, z_i)} \tag{3}$$

where $r'(\theta, z_i)$ and $r''(\theta, z_i)$ are the first and second derivatives of $r(\theta, z_i)$ with respect to θ.

Friction of the sock on the leg is neglected, which means that no tangential stress is considered.

2.4 Material properties

2.4.1 Constitutive equations

Soft tissues in regions one and two are defined as homogeneous, isotropic, near-incompressible and hyper-elastic materials. A Neo-Hookean strain energy function is used (Avril et al. 2010; Linder-Ganz et al. 2007). This energy function models the mechanical behaviour of the equivalent homogenized materials (material one for the region one and material two for the region two) where the properties are a mixture of the properties of the biological components of the regions. The Neo-Hookean strain energy function may be written:

$$W = \frac{G}{2}\left(\overline{I}_1 - 3\right) + \frac{K_v}{2}\left(J - 1\right)^2 \tag{4}$$

where $\overline{I}_1 = \mathrm{Tr}\left(\overline{\mathbf{F}}.\overline{\mathbf{F}}^t\right)$ is the first deviatoric strain invariant, $J = \det(\mathbf{F})$ the volume ratio, $\mathbf{F}$ the deformation gradient, $\overline{\mathbf{F}} = J^{-\frac{1}{3}}\mathbf{F}$ the deviatoric deformation gradient and Tr the trace of a matrix. The behaviour of each material is driven by two parameters: G_1 and K_{v1} for material one and G_2 and K_{v2} for material two. For infinitesimal deformations, K_v denotes the bulk modulus (or compressibility modulus) whereas G denotes the shear modulus. These constitutive parameters are identified by an inverse method which is detailed in the following paragraph.

2.4.2 Identification methodology

In order to determine the parameters G and K_v, an inverse method is used. Three steps are necessary:

(1) image warping using the FE model,
(2) mismatch estimation between the registered image and the target image,
(3) mismatch minimisation with the bounded Levenberg-Marquardt algorithm (BLVM) implemented in Matlab©.

Figure 4 below is an overview of the identification methodology employed.

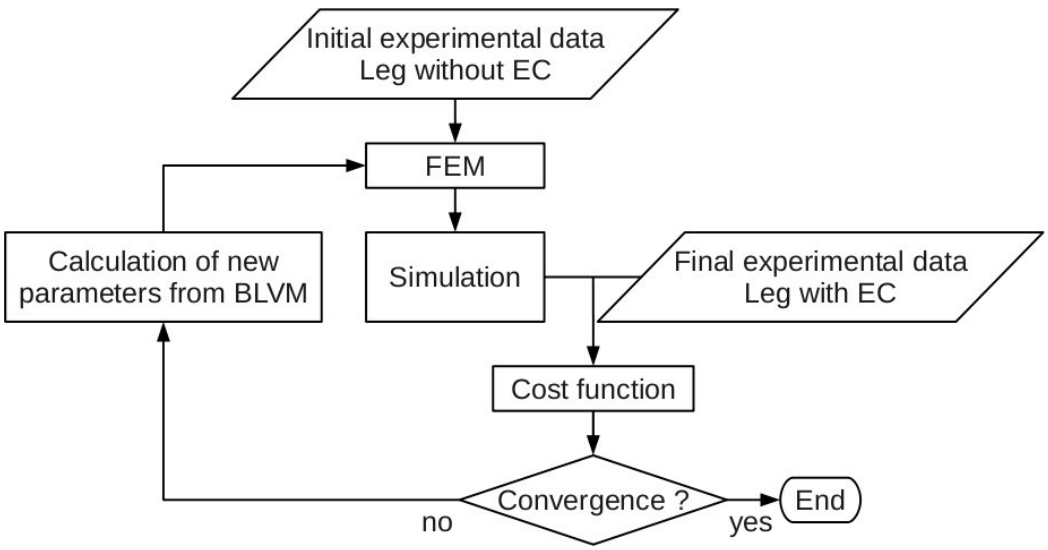

Figure 4. Optimisation algorithm by an inverse method.

Image warping. Before performing the image warping with the FE method, the two CT-scan images (with and without EC) need to be aligned in the same geometrical referential. For this purpose, the two images (respectively called the reference and the floating images) are registered with a rigid transformation following the Iterative Closest Point (ICP) scheme (Besl and McKay 1992). The 3D registration process is applied on the points of region three (bones) which is not deformable. The following steps are iterated until convergence:

(1) Pair each point of the floating image with the closest point of the reference image,
(2) Compute the transformation that will best superimpose the paired points,
(3) Apply this transformation to the points of the floating image.

After this operation, warping with the FE method may be achieved. Only the position of the nodes located across the external surface of the leg is considered.

- Let $(X,Y)^{init}$ denote the position of the nodes in the undeformed geometry obtained from the CT-scans of the leg *without* EC.
- Let $(X,Y)^{target}$ denote the position of the nodes in the deformed geometry obtained from the CT-scans of the leg *with* EC (after rigid registration).
- Let $(X,Y)^{simul} = (X,Y)^{init} + (u,v)$ denote the "virtual" position of the nodes after computing the deformation of the leg due to EC by the FE model.

The locations of $(X,Y)^{simul}$ and $(X,Y)^{target}$ are approximated by five-degree-Fourier descriptors (Equation 1) in 29 horizontal cross sections (one centimetre apart). Thus, for each cross section, the contours of the form $r^{simul}(\theta,z)$ and $r^{target}(\theta,z)$ are obtained respectively for the simulated and target data.

Mismatch estimation. The cost function to be minimized is constructed from the simulated and target contours of the leg.

The $r(\theta, z)$ function is used to build the following cost function (Figure 5):

$$\begin{aligned} C\left(G_1, K_{v1}, G_2, K_{v2}\right) &= \sum_{i=1}^{29} \int_0^{2\pi} \left[\frac{r^{simul}(\theta, z_i) - r^{target}(\theta, z_i)}{r^{target}(\theta, z_i)} \right]^2 d\theta \\ &= \sum_{i=1}^{29} Mis(z_i) \end{aligned} \tag{5}$$

where $Mis(z_i)$ is the mismatch between the simulated and the target data at height z_i.

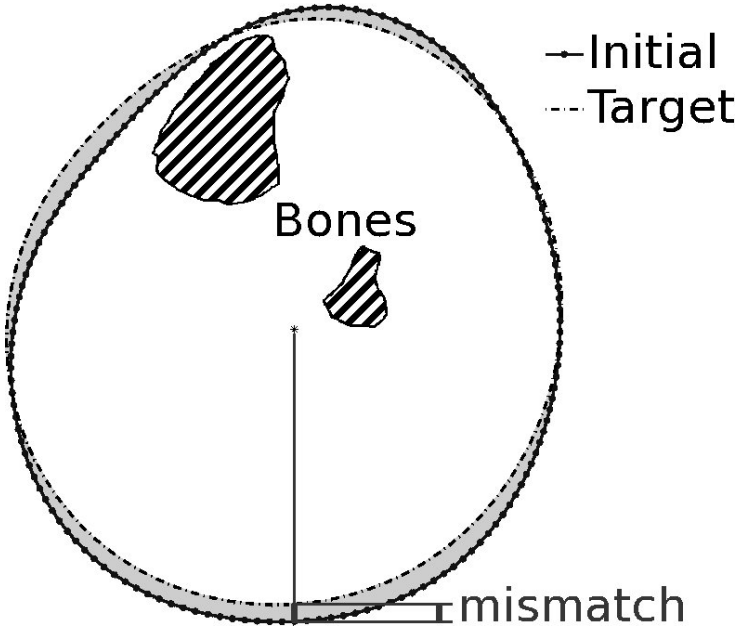

Figure 5. Mismatch number calculation to build the cost function C between the experimental target data and the initial data (the simulation initial condition).

Optimisation. The BLVM algorithm is used to minimize the cost function C defined above since it is dedicated to least-squares minimization problems. It requires computing the gradient of C with respect to the parameters, which is performed by backward finite differences.

The stopping criterion of the optimisation is the norm of the increments of the normalized parameters. It is fixed at 10^{-5}.

3. Results

3.1 External pressure map

The pressure applied by the sock onto the skin estimated using Equation 2 is shown on Figure 6. Large pressures are located at the middle of the tibia and on the gastrocnemius muscles, where the curvature radii are smaller. The pressure is null in zones where the curvature radii are negative because the sock does not compress them.

Figure 6. External pressure applied on the leg. Posterior, exterior, anterior, interior views and circumferential mean pressure.

3.2 Identified constitutive parameters

The initial values of the parameters used to start the optimisation are: $G = 20$ kPa; $K_v = 500$ kPa for both materials. The identified G coefficients are 11.1 kPa and 5.8 kPa, and the identified K_v coefficients are 1.06 MPa and 1.16 MPa respectively for material one and material two.

The strain energy function (Equation 4) consists of two terms which correspond to:

- a contribution of deviatoric strains arising from shape changes: $W_{isoch} = G(\overline{I}_1 - 3)/2$
- a contribution of volume changes: $W_{dilat} = K_v(J-1)^2/2$

In the Neo-Hookean model, each contribution is assigned a constant constitutive parameter. The order of magnitude of the bulk modulus K_v can be estimated according to:

$$K_v^{estim} = -V_0 \frac{\Delta P}{\Delta V} \tag{6}$$

where V_0 denotes the initial volume, ΔP the variation of pressure and ΔV the variation of volume. Knowing that the variation of volume of the leg is 0.5 % and knowing that the mean and maximum pressures are 2.5 kPa and 4.7 kPa, the value of the bulk modulus can be estimated to be around 460-870 kPa.

The values of the G coefficients found in literature range from 16 to 32 kPa for fat and 8 to 145 kPa for muscles (Linder-Ganz et al. 2007; Tran et al. 2005).

The values of material properties obtained from the identification procedure developed in this paper are of the same order of magnitude though the values are slightly different.

Figure 7 shows the initial, target and simulated contours (Fourier descriptors) at different heights. On the simulated contour, a colormap shows the mismatch for each cross section. The major mismatch of the contour is located at the interior side of the leg. These results are obtained after 30 hours of calculation and 12 BLVM iterations.

The mismatch number of the initial mesh is $C_{init} = 2.11$ and the one at the end of the simulation with the optimum constitutive parameters is $C_{optim} = 1.26$.

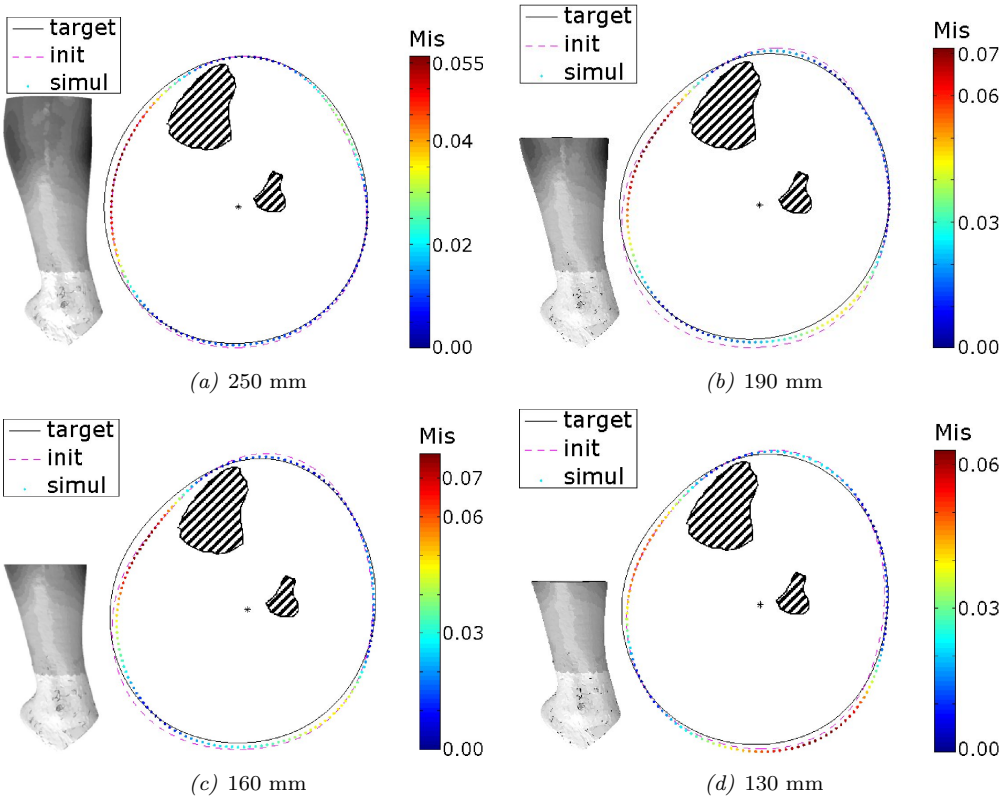

(a) 250 mm *(b)* 190 mm

(c) 160 mm *(d)* 130 mm

Figure 7. Initial, target and simulated contours of the leg, at cross sections located respectively at 250 mm (a), 190 mm (b), 160 mm (c) and 130 mm (d) from the ankle. The simulated contour is plotted using a colormap representing the mismatch with the target contour.

3.3 Pressure field

The way in which the pressure is transferred from the skin to the deep tissues is analysed. The hydrostatic pressure field inside the leg emphasizes a heterogeneous pressure distribution inside the leg (Figure 8). The maximum pressure is located where the curvature radius is minimum: near the tibia (on the front of the leg) and in the fat near the gastrocnemius muscles.

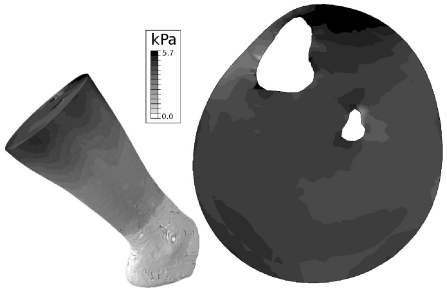

Figure 8. Hydrostatic pressure field inside the leg.

Figure 9 shows the hydrostatic pressure as a function of height at the main veins' locations in the deep and superficial venous system. This pressure is compared to

the average pressure applied. Due to the geometric effects and bones' locations, the hydrostatic vein pressure is found to be higher than the average applied pressure.

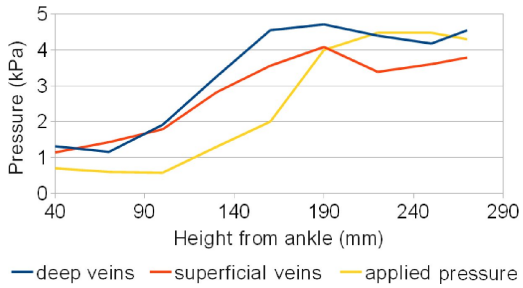

(a)

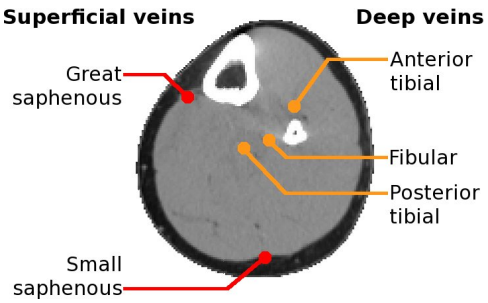

(b)

Figure 9. Mean computed hydrostatic pressure as a function of height (a). Main deep and superficial veins' locations (b).

4. Discussion

4.1 Comparison of 2D and 3D models

In previous 2D studies (Avril et al. 2010), the identification of the properties of soft tissues in leg was based on the images of a cross section of the calf, taken at the height where the perimeter of the calf is the largest. On this cross section, the area change between the uncompressed and the compressed state was 4.5%. The plane strain assumption which is common in 2D problems (Gefen 2002; le Floch et al. 2009), has also been used in this previous study. However the leg is very different from an infinite cylinder. Accordingly, 3D effects may be significant, justifying the 3D model developed in this paper.

An important aspect of the 2D *versus* 3D comparison is the dramatic difference observed between the area change of cross sections located at the top and at the bottom of the leg (see Figure 10). The maximal area change is 3.1%, in the cross section taken at mid-calf, *i.e.* at the location where the scans of the 2D model were acquired in Avril et al. (2010). Other cross sections have no change of area while some cross sections are subject to an increase in the area. The resulting volume change across the whole leg is 0.5% according to the 3D CT-scans.

Therefore, the 3D model is more adapted to the identification of tissue compressibility. In the 2D approach (Avril et al. 2010), the bulk modulus was underestimated. The relatively large shrinking of the leg in the considered cross section was actually compensated by swelling of the leg at other heights, making the total volume change less than 1%.

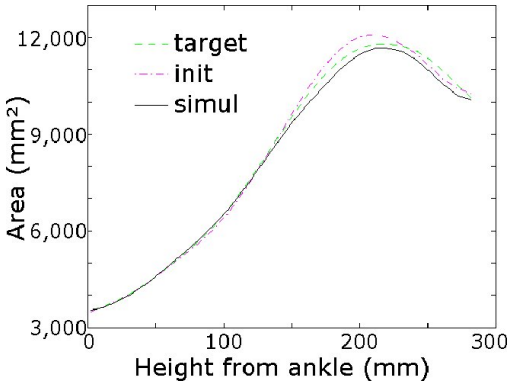

Figure 10. Initial, target and simulated cross sectional areas plotted as a function of height.

4.2 Relevancy of the model

External pressure from Laplace law. The external pressure applied onto the skin depends on the sock stiffness and on the curvature radii. Figure 11 shows the curvature radius as a function of the angular position at a height of 190 mm from the ankle. The shape of this graph is in agreement with those previously obtained by Gaied et al. (2006) and the pressure is of the same order of magnitude. It ranges between 0.5 and 4.5 kPa for Gaied et al. (2006) and 0.6 to 4.7 kPa for the present study.

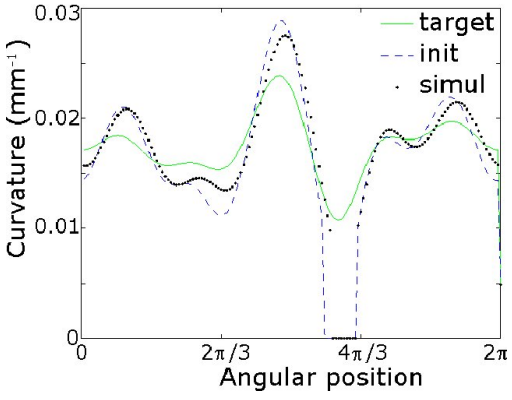

Figure 11. The curvature according to the angular position at 190 mm from de ankle for the initial, target and simulated contours.

Material properties. The constitutive model may therefore be discussed. Soft tissue properties are assumed isotropic and homogeneous. Although this is a common assumption for fat (Azar et al. 2002; Chung et al. 2008; Linder-Ganz et al. 2007; Tran et al. 2005), muscles are made up of fibres, which results rather in transversely isotropic material properties (van Loocke et al. 2006; Weiss 1994). Also the formulation of the strain energy function may not be suitable for this specific problem. Furthermore, fasciae and muscular compartments, which play a significant role in the mechanical response of the system, were not considered because another image modality such as MRI would be required to distinguish them.

Mismatch. The graph showing the curvature radius as a function of the angular position (Figure 11) is smoother for the target contour than the initial contour which means that the target is more rounded. From this point of view, the FE model

with identified parameters does not succeed in fitting properties in zones where $\left(r^{simul} - r^{target}\right)$ is negative. It is believed that friction between the sock and the skin may be important. The sliding between the different muscular compartments, and the transverse isotropy of the muscles can also have consequences on the results.

Finally, it might be helpful to make the cost function sensitive to additional changes in the leg. For instance, the expression of the cost function could also include the internal contour of the interface between materials one and two.

All these improvements in the model are out of the scope of this paper mainly dedicated to the inverse methodology. More sophisticated models will be considered in future studies.

4.3 Effects of the EC on the tissues

Consequence of non homogeneous pressure. Currently, the choice of a compression sock is based only on the calf size and on the disease significance (Partsch et al. 2006). However, the present study shows that the spatial variations of pressure are significant inside the leg and, consequently, pressure transmission through the internal tissues should be considered in treating venous disease. As an illustration, the pressure transmitted to the main veins of the leg is not obvious (Figure 8). A correction factor dedicated to estimating the pressure actually transmitted to veins, and depending on patient morphology, could help physicians to choose compression socks.

Note also that the mechanical role of veins was neglected in this first 3D model, the pressure applied onto the vein walls was assumed to be the same as the pressure in the surrounding tissues. This assumption could not be evaluated in the current study. A more complex model involving muscular contractions (to compare with Maton et al. (2006)) or fluid-structure interactions will be set up in the future to address this issue. Similarly, the effect of fasciae on the pressure distribution will be addressed.

5. Conclusion and perspective

For the first time, an inverse approach based on 3D images has been applied to identify constitutive properties of biological soft tissues in the leg. The paper has mainly been focused on the presentation of the inverse methodology and on its application to the problem of leg compression. Results prove the feasibility of the approach. Moreover, the model emphasizes large heterogeneities of the pressure distribution inside the leg. Future studies will consider more sophisticated models for the leg constituents in order to develop a patient-specific 3D FE model of the human leg under compression.

In order to take a step in the direction of medical exploitation of the model, improvements are currently under progress:

- consider anisotropy of the muscles,
- consider muscle compartments and fasciae,
- apply the method to other patients in order to understand the effect of the leg morphology.

Amongst the perspectives, it is also planned to include the veins in the model in view of simulating the mechanisms of venous return and the action of compression socks on venous flow in the human leg.

Acknowledgements

The authors are grateful to the Rhone-Alpes Regional Council for funding the Ph.D. grant of L.D and to the ANR (French National Research Agency) for its support. J-F Pouget and the Clinique Mutualiste de Saint-Étienne are gratefully acknowledged for their help with medical images, and BVSport© for providing and characterizing the socks.

References

6.9 Abaqus. *Abaqus Theory Manual*. ©Dassault Systèmes. 2009.

AFNOR. 1986. NF G30-102. Article de bonneterie - Détermination de la pression de contention

Amsler F, Willenberg T, Blättler W. 2009. In search of optimal compression therapy for venous leg ulcers: a meta-analysis of studies comparing divers bandages with specifically designed stockings. J Vasc Surg 50(3):668–674.

Aubert JT, Bassez S, Louisy F, Ribreau C. 2001. Accélérations dans le réseau veineux du membre inférieur au cours de la marche stationnaire. Paper presented at: *XVème Congrès Francais de Mécanique*. Marseille, France. Centre Universitaire Marseille Saint-Charles. pp. 3–7.

Avril S, Bouten L, Dubuis L, Drapier S, Pouget JF. 2010. Mixed Experimental and numerical approach for characterizing the biomechanical response of the human leg under elastic compression. ASME J Biomech Engrg 132(3):031006.

Azar F, Metaxas D, Schnall M. 2002. Methods for modeling and predicting mechanical deformations of the breast under external perturbations. Med Image Anal 6:1–27.

Besl P, McKay N. 1992. A Method for Registration of 3-D Shapes. IEEE Trans Pattern Anal Mach Intell 14(2):239–256.

Bouten L. 2009. Identification des propriétés mécaniques des tissus constitutifs du mollet pour l'étude mécanique de la contention [PhD thesis]. [Saint-Étienne (France)]: École Nationale Supérieure des Mines de Saint-Étienne.

Chung JH, Rajagopal V, Nielsen PMF, Nash MP. 2008. A biomechanical model of mammographic compressions. Biomechan Model Mechanobiol 7:43–52.

Couzan S, Assante C, Laporte S, Mismetti P, Pouget JF. 2009. Booster study: Comparative evaluation of a new concept of elastic stockings in mild venous insufficiency. Presse Med 38(3):355–361.

Cros F, Flaud P, Dantan P. 2002. A Digital Model for the Venous Junctions. Comput Meth Biomech Biomed Eng 5(6):421–429.

Dai X, Liu R, Li Y, Zhang M, Kwok Y. 2007. Numerical Simulation of Skin Pressure Distribution Applied by Graduated Compression Stockings. Stud Comp Intell 55:301–309.

Downie S, Raynor S, Firmin D, Wood N, Thom S, Hughes A, Parker K, Wolfe J, Xu XY. 2008. Effects of elastic compression stockings on wall shear stress in deep and superficial veins of the calf. Am J Physiol-Heart C 294(5):H2112–H2120.

Fung YC, Tong P. 2001. Classical and computational solid mechanics. Singapore: Word Scientific Publishing. Advanced Series in Engineering Science. Vol. 1.

Gaied I, Drapier S, Lun B. 2006. Experimental assessment and analytical 2D predictions of the stocking pressures induced on a model leg by Medical Compressive Stockings. J Biomech 39(16):3017–3025.

Gefen A. 2002. Stress analysis of the standing foot following surgical plantar fascia release. J Biomech 35(5):629–637.

Guesdon P, Fullana JM, Flaud P. 2007. Étude exprimentale du drainage musculaire. C R Mec 335(4):207–212.

leFloch S, Ohayon J, Tracqui P, Finet G, Gharib AM, Maurice RL, Cloutier G, Pettigre RI. 2009. Vulnerable atherosclerotic plaque elasticity reconstruction based on a segmentation-driven optimization procedure using strain measurements: theoretical framework. IEEE Trans Med Imaging 28(7):1126–1137.

Li Y, Zhang X, Yeung K. 2003. A 3D Biomechanical Model for Numerical Simulation of Dynamic Mechanical Interactions of Bra and Breast during Wear. Sen'i Gakkaishi 59(1):12–21.

Linder-Ganz E, Shabshin N, Itzchak Y, Gefen A. 2007. Assessment of mechanical conditions in sub-dermal tissues during sitting: A combined experimental-MRI and finite element approach. J Biomech Model Mechanobiol 40(7):1443–1454.

Maton B, Thiney G, Ouchene A, Flaud P, Barthelemy P. 2006. Intramuscular pressure and surface EMG in voluntary ankle dorsal flexion: Influence of elastic compressive stockings. J Electromyogr Kines 16(3):291–302.

Musani M, Matta F, Yaekoub A, Liang J, Hull R, Stein P. 2010. Venous Compression for Prevention of Postthrombotic Syndrome: A Meta-analysis. Am J Med 123(8):735–740.

Oduncu H, Clark M, Williams R. 2004. Effect of compression on blood flow in lower limb wounds. Int Wound J 1(2):107–113.

Oomens C, Bressers O, Bosboom E, Bouten C, Bader D. 2003. Can Loaded Interface Characteristics Influence Strain Distributions in Muscle Adjacent to Bony Prominences?. Comput Meth Biomech Biomed Eng 6(3):171–180.

Partsch H, Partsch B, Braun W. 2006. Interface pressure and stiffness of ready made compression stockings: Comparison of in vivo and in vitro measurements. J Vasc Surg 44(4):809–814.

Tran HV, Charleux F, Ehrlacher A, Ho Ba Tho MC. 2005. Propriétés mécaniques multi-couches de la peau humaine *in vivo*. Paper presented at: *7ème Colloque national en calcul des structures*. Giens, France. Université de Technologie de Compiègne.

vanDonkelaar CC, Huyghe JM, Vankan WJ, Drost MR. 2001. Spatial interaction between tissue pressure and skeletal muscle perfusion during contraction. J Biomech 34(5):631–637.

vanKaick O, Hamarneh G, Ward AD, Schweitzer M, Zhang H. 2010. Learning Fourier Descriptors for Computer-Aided Diagnosis of the Supraspinatus. Acad Radiol 17(8):1040–1049.

vanLoocke M, Lyons C, Simms C. 2006. A validated model of passive muscle in compression. J Biomech 39(16):2999–3009.

Weiss JA. 1994. A constitutive model and finite element representation for transversely isotropic soft tissues [PhD thesis]. [Utah (UT)]: University of Utah.

You F, Wang JM, Liao GJ. 2007. The Simulation of Elastic Human Body Deformation and Garment Pressure with Moving Mesh Method. Stud Comp Intell 55:289–300.

Zahn CT, Roskies RZ. 1972. Fourier descriptors for plane closed curves. IEEE Trans Comput c-21(3):269–281.

Zhang M, Dai X, Li Y, Cheung JM. 2007. Computational Simulation of Skin and Sock Pressure Distributions. Stud Comp Intell 55:323–333.